CrystEngComm

Accepted Manuscript

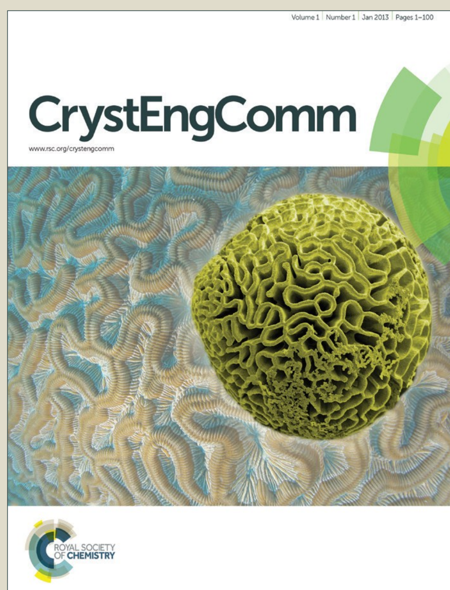

This is an *Accepted Manuscript*, which has been through the Royal Society of Chemistry peer review process and has been accepted for publication.

Accepted Manuscripts are published online shortly after acceptance, before technical editing, formatting and proof reading. Using this free service, authors can make their results available to the community, in citable form, before we publish the edited article. We will replace this *Accepted Manuscript* with the edited and formatted *Advance Article* as soon as it is available.

You can find more information about *Accepted Manuscripts* in the Information for Authors.

Please note that technical editing may introduce minor changes to the text and/or graphics, which may alter content. The journal's standard Terms & Conditions and the Ethical guidelines still apply. In no event shall the Royal Society of Chemistry be held responsible for any errors or omissions in this *Accepted Manuscript* or any consequences arising from the use of any information it contains.

ROYAL SOCIETY OF CHEMISTRY

www.rsc.org/crystengcomm

Highly elongated vertical GaN nanorod arrays on Si substrates with AlN seed layer by pulsed-mode metalorganic vapor deposition

Si-Young Bae[1, *], Byung Oh Jung[1], Kaddour Lekhal [1], Sang Yun Kim[2,3], Jeong Yong Lee[2,3], Dong-Seon Lee[4], Manato Deki[1], Yoshio Honda[1], and Hiroshi Amano[1,5]

[1]Department of Electrical Engineering and Computer Science, Nagoya University, Nagoya, Aichi 464-8603, Japan

[2]Center for Nanomaterials and Chemical Reactions, Institute for Basic Science (IBS), Daejeon 305-701, South Korea

[3]Department of Materials Science and Engineering, Korea Advanced Institute of Science and Technology (KAIST), Daejeon 305-701, South Korea

[4]School of Information and Communications, Gwangju Institute of Science and Technology (GIST), Gwangju 500-712, Korea

[5]Akasaki Research Center (ARC), Nagoya University, Nagoya, Aichi 464-8603, Japan

Abstract

To extend the availability of nanostructure-based optoelectronic applications, vertically elongated nanorods with precisely controlled morphology are required. For the group III nitrides, pulsed-mode growth has recently been reported as an effective method of growing nanorod arrays with geometric precision. Here, we demonstrated the growth of arrays of highly elongated nanorods on Si substrates by metal-organic chemical vapor deposition with using pulsed-mode approach. Unlike the thick and high (or middle)-quality GaN templates normally used, nanorod growth was performed on an ultrathin and low-quality AlN/Si platform. Using kinetically controlled growth conditions and a patterning process, exceptionally long GaN nanorods were achieved with high geometric precision. The grown nanorods showed considerably improved optical and structural properties while remaining in uniform arrays. This approach can be used with a variety of materials to obtain nanorods with high quality, high uniformity, and high aspect ratio, and it can also serve as an effective fabrication method for InAlGaN-alloyed core/shell nanostructures for optoelectronic nanodevices with ultrahigh efficiency.

CrystEngComm Accepted Manuscript

Keywords: nanorod array, GaN on Si, AlN seed layer, pulsed-mode growth, and metalorganic chemical vapor deposition

* Corresponding author: Si-Young Bae; E-mail: siyoubae@gmail.com; Tel.: +81-52-789-5275; Fax: +81-52-789-3156

Introduction

Nanostructures in solid-state semiconductors have received wide interest in the search for novel applications in optoelectronic, thermoelectric, and magnetic fields.[1] In particular, for group III nitride systems, several merits of nanostructures are expected: the removal of the quantum-confined Stark effect, the reduction of threading dislocation density, the relaxation of epitaxial strain, an increased emission area to obtain a high output power, high indium incorporation, and spectrum broadening for phosphor-free white emission.[2–6] Furthermore, much smaller scale nanostructures of group III nitrides have been of interest since they may allow coverage of the entire visible spectral range.[7,8] For these reasons, GaN nanostructures may be a promising means of enhancing the quantum efficiency of bandgap-controlled optoelectronic devices even in green and red ranges.

For the synthesis of elongated GaN nanostructures, i.e., nanowires or nanorods, several methods have been developed over the past few decades. Catalytic and template-assisted approaches, such as molecular beam epitaxy (MBE), metal-organic chemical vapor deposition (MOCVD), hydride vapor phase epitaxy (HVPE), and so forth, have been employed in various epitaxy systems.[9–11] For these systems, vapor-liquid-solid (VLS) growth has become the most popular method of growing nanowires—under the eutectic melting temperature of catalytic metals, the supersaturation of liquid droplets promotes local crystallization on nuclei sites.[11] VLS growth enables the formation of exceptionally elongated GaN nanowires with a high growth rate and multiple directionality.[11,12] Recent advances in GaN VLS growth have enabled the growth of horizontally well-aligned nanostructures, thereby providing a new means of controlling the directionality of nanostructures.[13] However, these approaches do not yet fulfill the requirements for geometrically precise arrays in

CrystEngComm Accepted Manuscript

terms of their length, diameter, density, and uniformity.

One attractive approach to obtaining geometrically well-aligned GaN nanostructures is to use selective area growth in which openings in masks typically serve as preferential nucleation sites for adatom absorption.[14] Then, the controlled growth of GaN nanostructures can be achieved in accordance with the patterning parameters such as shape, size, and density. To form such nanoscale patterns at a low cost and large scale, many patterning methods have been attempted: silica nanosphsere patterning, porous anodic alumina (PAA) patterning, laser interference lithography, nanoimprint, and so forth.[15,16] By employing preferentially well-oriented templates (e.g., GaN/sapphire or GaN/Si) underneath the mask pattern, regrown structures can have a highly preferential orientation, indicating the formation of GaN with three dimensional (3D) well-aligned in-plane geometry.[17] Indeed, vertically elongated GaN nanorods with high density have been successfully grown by MBE.[18] However, pyramidal GaN structures rather than GaN nanorods have been typically formed by selective area growth via MOCVD owing to strong hydrogen passivation on the semipolar surfaces.[19]

For the case of MOCVD, a breakthrough enabling the growth of vertically elongated GaN nanorod arrays has been achieved by employing *pulsed-mode growth*.[20] Since this breakthrough, several groups have attempted to improve the quality of GaN nanorods grown by MOCVE with the pulsed-mode approach.[5,21–24] Furthermore, the growth mechanisms of GaN nanorods have been revealed from their morphological evolution with the aim of precisely controlling their geometry.[25,26] Very recently, the feasibility of device applications based on GaN nanorod arrays was also demonstrated.[5,27] The important common ground in these approaches is the use of a high (or middle)-quality GaN template with a regular pattern as a mother layer (or seed layer) for selective area growth. Since the structures grown on the template are determined by the quality of the mother layer, it may be questioned whether pulsed-mode growth can still be effectively carried out on low-quality templates with nanoscale thickness (< 100 nm) and/or similar seed materials.[17] Once the feasibility of growing GaN nanorod arrrays on the ultrathin templates has been proved, several benefits can be expected in Si-based GaN epitaxy: (1) the availability of templates for physical deposition methods such as AlN

CrystEngComm Accepted Manuscript

sputtering;[28] (2) direct growth without strain relaxation layers (a stack of AlGaN layers is commonly used); (3) optical selectivity from the mother layer because of the large bandgap difference; (4) the realization of advanced device structures on nanoarray platforms such as novel III nitride/silicon tandem solar cells and vertical field-effect transistors.[29,30] In particular, the first and second benefits reduce costs owing to cheaper maintenance and simplified epilayers. However, there have been insufficient reports on the growth of GaN nanorods such ultrathin templates and the maximum length of GaN nanorods that can be grown using the pulsed-mode approach. Moreover, it is necessary for GaN nanorod arrays to have a micrometer-scale length (> 10 μm) and high crystal quality and to be grown in a highly controlled manner to ensure their commercial availability in the near future.

Therefore, in this paper, we report arrays of highly elongated and vertically aligned GaN nanorods grown on Si (111) substrates by MOCVD with the pulsed-mode approach while controlling the kinetic parameters, where an ultrathin AlN layer was adopted as a Si-based template. It was found that GaN nanorods with high crystal quality and a strong preferential orientation were successfully grown. We also studied kinetic Wulff plots and carried out volumetric analysis, which can provide a useful guide to growing arrays of even longer GaN nanorods.

Experimental

Template preparation: A 50-nm-thick AlN epitaxial layer on a Si (111) substrates was prepared as a basal template. It was grown using a commercial MOCVD system (SH4001-HTA, EpiQuest) and the detailed growth procedure is as follows. 2-inch Si substrates were heated to 1140 °C at a reactor pressure of 50 Torr in hydrogen (H_2) ambient. In this heating step, ammonia (NH_3) was not used to prevent the formation of a Si_3N_4 layer. When the substrate temperature reached 1140 °C, trimethylaluminium (TMAl) was injected for 10 s, but no NH_3 was used in this step. Subsequently, NH_3 was injected for 5 min to grow an AlN binary layer, where the TMAl and NH_3 flow rates were maintained at 100 sccm (197 μmol/min) and 700 sccm (31.3 mmol/min), respectively. To fabricate a dielectric mask array by selective-area growth, a 30-nm-thick SiO_2 layer was deposited on the AlN template by RF magnetron sputtering (ACS-4000-UHV-C3, ULVAC). Subsequently, spin coating

CrystEngComm Accepted Manuscript

with a polymer resin (MR-I 7020E imprint polymer, Micro resist technology) and thermal nanoimprinting (X-500, Scivax) were performed to form a circular hole array pattern, in which three types of nanoimprint pattern were utilized with diameters/pitch-to-pitch distances of 230/460 nm, 460/1380 nm, and 190/920 nm. Then, the SiO_2 layer was etched by reactive ion etching (RIE) with a CF_4 mixture gas. The residual polymer resin on the surface was completely eliminated by O_2-based plasma ashing and cleaning in aceton.

Nanorod growth process: After preparing a SiO_2 nanomask on the AlN/Si template, GaN nanorods were grown using the pulsed-mode method in MOCVD. The temporal sequence of valve operation in the MOCVD system is presented in Fig. S1. One cycle of the pulsed-mode sequence is composed of four steps: TMG ON (t_1), NH_3 ON (t_2), post-TMG OFF (t_3), post-NH_3 OFF (t_4). For the injection steps (ON steps), a TMG flow of 15 sccm (78 μmol/min) and an NH_3 flow of 5 slm (223.21 mmol/min) were typically used with pure H_2 as the carrier gas. The typical growth temperature was maintained at 1000–1020 °C and no dopant was used in this study. Depending on the growth conditions, the injection times (i.e., t_1, and t_2) were controlled by fixing the interruption times (i.e., t_3, and t_4). For the samples subjected to transmission electron microscopy (TEM) analysis, additional InGaN/GaN core-shell capping was performed, where triethylgallium (TEG), trimethylindium (TMI), and NH_3 were utilized as Ga, In, and N sources, respectively. Also a growth temperature of 770 °C was used in nitrogen (N_2) ambient. The reactor pressure was maintained at 200 Torr during the entire growth procedure. Details of the pulsed-mode growth procedure have also been described elsewhere.[5,26]

Characterization: The surface morphology of the samples was investigated by field-emission scanning electron microscopy (FE-SEM, S-5200 or SU70, Hitachi) with an operating voltage of 5 kV and by the atomic force microscopy (AFM, NanoNavi IIs, SII NanoTechnology). The crystalline orientation of the GaN nanorod arrays was characterized using an EBSD system (INCA Crystal EBSD system, Oxford Instruments) in the FE-SEM at 20 kV with a working distance of 15 mm and a sample tilt of 70°. Other crystalline properties were analyzed by an X-ray diffraction (XRD, X'pert

CrystEngComm Accepted Manuscript

Pro MRD, PANalytical) with Cu K_{α} radiation. Microstructural properties were characterized by TEM (Cs-corrected STEM, ARM200F) using a nanorod specimen fabricated by a dual-beam focused ion beam (DB-FIB, NOVA 200). Optical emission properties were studied by the investigation of their photoluminescence (PL) using the 325 nm line of a He-Cd laser at room temperature.

Results and Discussion

Morphology evolution in terms of pulsed-mode growth ratio

Once the growth temperature is fixed in pulsed-mode growth, the source modulation duration, i.e., the ON/OFF time, is of critical importance in maintaining the vertical rodlike morphology. For instance, too Ga-rich conditions because of a long TMG injection time can be adjusted to the optimum GaN growth condition by increasing the post-Ga interruption time, while a N-rich condition can be compensated by increasing the post-N interruption time as previously reported.[26] However, these approaches are somewhat ineffective in terms of the growth time since a Ga-rich (or N-rich) condition can be controlled by simply shortening the corresponding source injection time. Hence, to determine the optimum growth duration in this study, we only focus on the TMG and NH_3 injection times by fixing the post-interruption time (i.e., t_3 and t_4) to 1 s. In particular, we consider one temporal term, pulsed-mode growth ratio (PMGR), to make a common comparison for both the TMG and NH_3 injection times by defining PMGR = $(t_2/t_1)/(t_4/t_3)$, where t_1, t_2, t_3, and t_4 are the TMG injection time, NH_3 injection time, post-TMG interruption time, and post-NH_3 interruption time, respectively (see also the schematic procedure in Fig. S1).[26] Hence, in this study, PMGR simply refers to t_2/t_1 since t_4/t_3 = 1. First, GaN nanostructures grown with different NH_3 injection times were investigated with the TMG injection time fixed at 5 s. Cross-sectional SEM images of nanostructures grown with NH_3 injection times of 5 s, 10 s, and 20 s are shown in Figs. 1a–1c, respectively, i.e., PMGRs of 1, 2, and 4. For an NH_3 injection time of 10 s (Fig. 1b), vertically well-aligned nanorods were grown with partial semipolar surfaces in the topmost regions. The uniform orientation of the nanorods was almost perfectly maintained for all nanorods. Moreover, most of the nanorods had a relatively uniform size with a height in the range of 595–710 nm and a diameter of ~275 nm. Detailed length distributions

CrystEngComm Accepted Manuscript

along the vertical and lateral directions are displayed in Fig. S2a. For a short NH_3 injection time of 5 s (Fig. 1a), on the other hand, somewhat shorter nanorods were grown, that had not only a broad length distribution along both the vertical and lateral directions but also reduced semipolar surfaces in the topmost regions. In contrast, a long NH_3 injection time of 20 s (Fig. 1c) resulted in coalesced structures with the 30-nm-thick SiO_2 mask pattern clearly visible as marked by an arrow. This coalescence is attributed to the small distance (~230 nm) between the holes as well as enhanced lateral growth.

In a similar manner to the change in the NH_3 injection time, GaN nanostructures grown with different TMG injection times were subsequently investigated with the NH_3 injection time fixed at 15 s. Cross-sectional SEM images of the nanostructures grown with TMG injection times of 3.75 s, 5 s, 7.5 s, and 15 s are shown in Figs. 1d–1g, respectively, i.e., with PMGR decreasing from 4 to 1. We found that the optimum growth of vertically well-aligned nanorods occurred with NH_3/TMG injection times of 15 s/5 s (Fig. 1e). The nanorods had semipolar surfaces in the topmost regions as similarly observed in Fig. 1b. Figure S2b presents detailed length distributions of the grown GaN nanostructures for different TMG injection times. When t_I was 5 s, clearly improved uniformity in terms of the size distribution and a nanorod height of ~730 nm and diameter of ~330 nm were observed. It can be seen that as the TMG injection time increased from the optimum value, the height distribution became much broader. Increasing the TMG injection time promoted the formation of disordered GaN nanostructures and partially coalesced structures, as shown in Fig. 1g. Moreover, the individual top surfaces were almost flat, indicating suppression of the formation of semipolar GaN surfaces. However, some nanorods had a similar or even greater height than the optimized GaN nanorods owing to the sufficient TMG injection time. On the other hand, for the short TMG injection time of 3.75 s (Fig. 1d), short GaN nanorods with an increased diameter were grown. Hence, we could determine the optimized growth conditions for GaN nanorods with a high aspect ratio of ~3 from the morphology as well as the size distribution.

These results clearly indicate that the ratio of the source injection times, i.e., PMGR, plays an important role in controlling the GaN nanorod morphology. The mechanism behind the change in the

CrystEngComm Accepted Manuscript

morphology can be explained by the control of the growth rate on the different facets.[31] Without pulsed-mode operation (i.e., continuous-mode growth), nanoscale selective-area growth results in a pyramidal morphology typically composed of $\{10\bar{1}1\}$ and $\{11\bar{2}2\}$ surfaces.[32,33] According to kinetic Wulff growth theory, these surfaces can be determined owing to the lowest growth rate of the resultant planes.[34,35] In particular, in the case of Ga-polar GaN structures, the strong hydrogen passivation effect via N–H bonding on the N-terminated surfaces can contribute to the low growth rate, thereby promoting the growth of $\{10\bar{1}1\}$ semipolar surfaces.[19] Moreover, we used an AlN buffer layer as a seed layer, indicating that Ga-polar GaN can be easily grown owing to the Al platform of top surfaces.[36] Note that PMGR of ~3 was found to result in the optimum growth in our study. We believe that this condition provides sufficient Ga flux to induce unstable N–H passivation surfaces, thereby resulting in vertically well-aligned Ga-polar GaN nanorods.[19] Lower PMGR values (< 2) result in too high Ga flux. Hence, the topmost semipolar surfaces on nanorods disappeared and a wide range of heights was observed (see Figs. 1a and 1g). On the other hand, a higher PMGR (> 4) can induce a N-rich ambient. At the same time, a large number of hydrogen atoms can be decomposed from NH_3, thereby resulting in strong hydrogen passivation on the topmost $\{10\bar{1}1\}$ semipolar surfaces from the planes with the lowest growth rate (see Fig. 1d).

Photoluminescence and structural properties of nanostructures

To obtain the optimized nanorod structures in terms of optical properties as well as their morphology, PL measurements were carried out on the grown nanostructures. Figures 2a and 2b show the room-temperature PL spectra of GaN nanostructures for different values of t_1 and t_2. Here, a He-Cd laser with a wavelength of 325 nm was used for excitation and the exposure time was 100 ms. First, the dependence of the PL properties on the NH_3 injection time is displayed in Fig. 2a. As can be seen, GaN nanorods with PMGR of 2 (t_2/t_1 = 10 s/5 s) exhibit excellent band-edge (BE) intensity at ~365.7 nm. Moreover, defect-related yellow luminescence was almost completely suppressed, resulting in a high BE/YL ratio of > 100. Non-optimized conditions, on the other hand, resulted in very weak BE intensity of the grown GaN nanostructures with a relatively low BE/YL ratio. Note that these PL

CrystEngComm Accepted Manuscript

emission properties could be easily separated from those of the AlN buffer layer since the band energy of the latter is high compared with the GaN BE energy. Hence, the strong PL intensity of the GaN in this study can be *directly* attributed to the high crystal quality of the GaN nanorods without any signals from the mother layer. This may be a significant merit of AlN templates compared with previously used GaN templates. We observed very similar behaviors for the TMG injection time dependence of GaN nanostructures in Fig. 2b. In particular, the optimized GaN nanorods with PMGR of 3 (t_2/t_1 = 15 s/5 s) exhibited the strongest BE intensity with almost no yellow luminescence. Similar but slightly lower PL intensity was observed for the GaN nanorods with PMGR of 4 (t_2/t_1 = 15 s/3.75 s) owing to their lower height. It can also be seen that as the TMG injection time increases from the optimized condition, the BE intensity decreases rapidly. For all samples, the peak intensity was located at ~365.7 nm, indicating that the grown GaN nanostructures have almost strain-free BE emission.[37] This means that the GaN nanorods might relax the residual tensile strain generated at the beginning of the growth process in a similar manner to previously reported rodlike GaN structures.[38] Also the growth rate was lower than that of VLS growth reported elsewhere, indicating that the pulsed-mode growth is governed by typical vapor phase epitaxy.[9,11,12]

Together with these PL properties, we investigated the microstructural properties at the interfaces by TEM analysis. Figure 2c shows a dark-field (DF) TEM image of grown GaN nanorods with outer InGaN/GaN shells with a hole diameter of 230 nm after 150 pulsed-mode cycles. The image correctly reflects the stack comprising Si/AlN layer/SiO_2 mask/GaN nanorods. Although slightly spiky structures were observed at the interplane corners between pyramids and sidewalls, they are attributed to the change in the growth mode from the pulsed mode to the continuous mode during the growth of the shells. We observed hardly any dislocation features in the GaN nanorods, indicating their high quality. The mechanism behind the elimination of threading dislocations has been discussed elsewhere; dislocations may have been bent as a result of a reduction in the dislocation line energy.[24] The extent to which defects can appear in the mother layer used for the pulsed-mode growth of GaN nanorods is of interest because of the prominent use of high-quality GaN templates so far. This study considers the extreme case of an AlN seed layer (see Fig. S3 for its material properties) with a high

CrystEngComm Accepted Manuscript

defect density at the AlN/Si interface, as shown by its disordered atomic arrangement (Fig. 2f), with a slightly rough morphology. Clear evidence for the elimination of threading dislocations was found on another similar GaN nanorod structure with a larger hole diameter of 460 nm in Fig. 2d. A high dislocation density was clearly observed on the AlN layer and some dislocations propagated from the AlN layer to the GaN core region. However, all the dislocations in the GaN core region were blocked or bent in the middle of the nanorods. Hence, we could achieve dislocation-free GaN noanorods in the topmost region. This dislocation filtering effect predominantly occurred within a few hundred nanometers from the bottom of the nanorods as reported elsewhere.[39] Therefore, we can grow dislocation-free GaN by further increasing the length of the nanorods. Figure 2e shows an XRD omega scan of the GaN nanorods with PMGR of 3. The full width at half maximum (FWHM) of omega scan was 212 arcsec, indicating similar or higher crystal quality than that of common two dimensional (2D) GaN/Si. Note that the FWHM of the XRD rocking curve of the AlN layer was evaluated to be 1.72°, indicating low crystal quality (Fig. S3c). Typical crystal growth evolves from these defective nuclei to form a high-quality layer.[40] Moreover, it is well known that the AlN layer plays a key role in effectively growing a high-quality GaN layer on heteroepitaxial substrates.[41] We observed that the AlN layer had a well-aligned in-plane crystal orientation (Fig. S3d) and ordered atomic features as growth proceeded, as shown in Fig. 2g. Owing to the effective role of the AlN layer, wurtzite GaN started to grow at the GaN/AlN interface, while poor ordering was found at the beginning of the growth (Fig. 2g). Finally, reasonably well aligned wurtzite GaN was achieved as the pulsed-mode growth proceeded, as shown in Fig. 2h. The inset of Fig. 2h confirms the formation of single-crystal wurtzite from the selective-area diffraction (SAED) pattern. It is necessary to separate this growth from the other VLS growth, in which stacking faults are commonly formed with a high density owing to the high growth rate.[42] The high growth rate can usually be taken into account by considering the promoted supersaturation of kinetic adatoms on nuclei.[9,11] On the other hand, these features were hardly observed in our nanorods, but a typical atomic arrangement similar to that of thin films was observed. Hence, we believe that the pulsed-mode growth can be explained using the

CrystEngComm Accepted Manuscript

classical film growth mechanism, where the kinetic parameters of the growth critically affect the equilibrium shape of the grown structures.

V/III ratio dependence and preferential orientation of nanorod arrays

Even though we have determined the optimized growth conditions in terms of the morphology and optical properties, a change in PMGR might sometimes be understood as a change in the V/III ratio. In fact, we could *not directly* calculate the V/III ratio during the pulsed-mode growth since each step in the growth sequence has a considerably different value owing to the altered source conditions. For example, the V/III ratio during Ga injection can be considered to be zero, while that during N injection can be considered to be infinite. Nevertheless, a simple approach to evaluating the V/III ratio in pulsed-mode growth is to assume that the Ga and N sources were injected at the same time in a similar manner to in continuous-mode growth. Figures 3a–3c show SEM images of nanostructures grown while directly changing the V/III ratio from 1430 to 4290 using the continuous-mode-like concept. Note that except for the V/III ratio, the other growth conditions were identical to those for a PMGR of 3. Here, we adjusted the NH_3 flow to change the V/III ratio while keeping the TMG flow fixed. The V/III ratios of 1430, 2860, and 4290 corresponded to PMGRs of 1.5, 3, and 4.5, respectively. Major changes in the morphology compared with the case of changing the PMGR were observed. Here the grown morphologies were compared in terms of the two main growth directions on the equilibrium shapes, i.e., the vertical direction (*c*-plane) and lateral direction (*m*-plane or *a*-plane). Almost isotropic growth behavior in the two main directions was observed for the low V/III ratio (= 1430), as shown in Fig. 3a. On the other hand, vertically and laterally elongated structures were grown at the intermediate V/III ratio (= 2860) and high V/III ratio (= 4290), although slightly nonuniform structures were found owing to the lack of balance between the Ga and N adatoms for the high V/III ratio. To conceptually illustrate these behaviors, simple schematics are also included as insets in Figs. 3a–3c with arrows indicating the relative vertical length (L_v) and lateral length (L_l). These V/III ratio dependences are also comparable to that for a planar thin film. Figure 3d plots the ratio of N to Ga desorption k_N/k_{Ga} versus temperature reported by Koleske *et al*.[43] The line has the

CrystEngComm Accepted Manuscript

equation $k_N/k_{Ga} = 1.9205\times10^{16}\times\exp[-39563/T(\mathrm{K})]$.[43] High-quality thin films with a mirrorlike morphology were typically obtained with a k_N/k_{Ga} ratio 1.2 times higher than that based on the kinetic balance model.[43] Here, we marked the three V/III ratios used in this experiment in red circles. Figure 3d thus shows that a somewhat higher V/III ratio is applied for pulsed-mode growth compared with that for a typical thin film. Note that in the case of a planar thin film, Ga droplet-like structures are typically grown for a low V/III ratio, whereas Ga-vacancy-like structures are obtained for a high V/III ratio. These features can also be correlated to the enlarged nanostructures along both the vertical and lateral directions in Fig. 3a since a high density of Ga atoms was supplied at the low V/III ratio. On the other hand, the lack of N open sites at the high V/III ratio, i.e., N site blocking, might result in a decrease in the growth rate in the vertical direction. We believe that such N site blocking can also affect the pulsed-mode procedure since there is not only a lower growth rate but also a higher V/III ratio than those for typical planar growth. Thus, we can conclude that these changes in the direct V/III ratio severely affect the nanorod morphology owing to the changes in the amounts of V and III sources. Hence, changing PMGR during pulsed-mode growth should be considered as an elaborate means of using the residence times of V and III sources at a fixed V/III ratio rather than directly changing the V/III ratio itself. Changing PMGR in this manner could be used as a correction factor to control the nanorod morphology, as we reported elsewhere.[26] Even though the PMGR does not directly correspond to the V/III ratio, they might be strongly related. For example, a high PMGR (> 4) can be correlated to the high V/III ratio, thereby resulting in vertical growth with a pyramid-like morphology. On the other hand, a low PMGR can be correlated to the low V/III ratio, thereby increasing the Ga residence time since the low V/III ratio resulted in a high Ga density on the surface. This morphological functionality is reasonably effective provided that the range of conditions under which optimized pulsed-mode growth occurs is determined. We also explored the in-plane and out-of-plane preferential orientations for fixed pulsed-mode growth conditions. A top-view SEM image of the grown nanorods is shown in Fig. 3e. The two main in-plane orientations are marked as the $\langle 11\bar{2}0\rangle$ and $\langle 10\bar{1}0\rangle$ directions. We observed that each nanorod surface has strong coherence along the in-plane directions. Clear evidence of the crystal orientation was obtained from the electron

CrystEngComm Accepted Manuscript

backscatter diffraction (EBSD) pole figures in Fig. 3f, which show not only highly directional growth along the out-of-plane direction (*c*-plane) but also sixfold symmetric features along in-plane directions such as $\{10\bar{1}0\}$ and $\{10\bar{1}1\}$. Figure 3g provides a more quantitative analysis of these preferential orientations in the form of histograms of the tilted deviation angle. The maximum tilted deviation angles were 4.5° and 1.6° for the in-plane and out-of-plane orientations, respectively. Note that the coherent symmetries of the GaN nanorods are attributed to the strong preferential orientations of the AlN buffer layer despite its low crystal quality (Fig. S3). Hence, the crystallographic orientation of the mother layer is the most important factor in ensuring the geometrical precision of GaN nanorods rather than its quality or residual strain.

Kinetic Wulff plot of GaN nanorods

To clarify the above arguments in detail, we examined the equilibrium shapes and their kinetic Wulff plots for three representative equilibrium shapes observed in this study: a hexagonal pyramid, short nanorod, and long nanorod (Fig. 4). Indeed, these nanostructures with faceted shapes are commonly affected by several kinetic factors (e.g., temperature, pressure, V/III molar flow, and so forth) under continuous-mode growth as well as pulsed-mode growth. Furthermore, as observed experimentally, pulsed-mode growth can induce the exceptional elongation of nanorods along the vertical direction, thereby critically affecting the growth rate on different surface planes. To fairly compare these growth behaviors, a kinetic Wulff plot (sometimes called a ν-plot) can be useful when the relative ratio of the growth rates is known.[44] Then, the equilibrium shapes can be represented by a full cusp (also called a discontinuity in the slope in two directions) in the ν-plot owing to the low growth rate of the specific equilibrium orientation. In our case, the selectively grown nanostructures enabled us to justify the growth rate obtained for each stabilized surface orientation from the faceted nanostructures that appeared. Once the key components of the ν-plot are determined, such as the growth rates of the *c*-, *m*-, *a*-, and $\{10\bar{1}1\}$ planes, we can estimate the values for the other missing orientations since they might have higher growth rates than the equilibrium shapes. To complete the ν-plot over the entire

CrystEngComm Accepted Manuscript

range of surface orientations, we performed interpolation using the following trigonometric function:[45]

$$v(\theta) = v_j \left| cos\left(\frac{\pi}{2(\theta_i - \theta_j)}(\theta - \theta_j)\right)\right| + v_i \left| sin\left(\frac{\pi}{2(\theta_i - \theta_j)}(\theta - \theta_j)\right)\right| \quad \theta_j \le \theta \le \theta_i ,$$

where $v(\theta)$ is the growth rate of any surface orientation at θ. θ_i, θ_j,.. and v_i, v_j,.. are the angles and growth rates at the position of the full cusp, respectively. A schematic of each shape and an actual SEM image are exhibited on the left side of each panel in Fig. 4. The growth length for the *c*-, *m*-, and *a*-plane surfaces was directly obtained from cross-sectional and top-view SEM images. In the case of the $\{10\bar{1}1\}$ plane surfaces, the growth length was acquired as the distance from the origin to a line drawn by linear interpolation along the partially appearing $\{10\bar{1}1\}$ semipolar facets (see also Fig. S4). Note that half ($0 \le \theta \le \pi$) of the full orientation range was considered in this study since only the *c*-plane side of the template was applicable. In addition, we could not observe any growth features of the opposite N-polar nanorods over the whole of each surface. The cross section of the ν-plots at the *m*-plane is shown on the right side of each panel in Fig. 4. Owing to the isotropic geometry, the plots are shown in the range of $0 \le \theta \le \pi/2$. These plots correctly illustrate the major features of the hexagonal nanostructures by showing three full cusps in the $[0001]$, $[10\bar{1}1]$, and $[10\bar{1}0]$ directions. As predicted, the deepest cusp along the $[10\bar{1}1]$ direction was found for the hexagonal pyramid structure in Fig. 4a. In other words, the other cusps in the $[0001]$ and $[10\bar{1}0]$ directions were shallower than that in the $[10\bar{1}1]$ direction, with the depth decreasing in the order $\nu_{0001} > \nu_{10\text{-}10} > \nu_{10\text{-}11}$. As shown in Fig. 4b, on the other hand, the short nanorod has the deepest cusp in the $[10\bar{1}0]$ direction with the depth decreasing in the order $\nu_{0001} > \nu_{10\text{-}11} > \nu_{10\text{-}10}$. The reverse order of the growth rates for the $[10\bar{1}1]$ and $[10\bar{1}0]$ directions was in reasonably good agreement with the partially grown *m*-plane equilibrium shapes in Fig. 1d. Figure 4c depicts much deeper cusps in the $[10\bar{1}0]$ direction for the long nanorod than for the short nanorod. Owing to the very different depths in the $[10\bar{1}1]$ and $[10\bar{1}0]$ directions, the *m*-plane equilibrium shape was more prominent than that of the other planes. Hence, pulsed-mode growth not only breaks the passivated hydrogen bonds on semipolar surfaces but also effectively suppresses the *m*-plane growth rate.

CrystEngComm Accepted Manuscript

Vertically elongated GaN nanorods obtained by increasing number of pulsed-mode cycles

As discussed for the kinetic Wulff plots of the GaN nanostructures, we predicted that optimized pulsed-mode growth can produce vertically well-elongated GaN nanorods. To experimentally extend this concept, as the next step, we observed the growth morphology of GaN nanorods with increasing growth time. Figures 5a–5f show SEM images of the GaN nanorods grown with the number of pulsed-mode cycles varied from 164 to 1000 for hole diameters of 460 nm (Figs. 5a–5c) and 190 nm (Figs. 5d–5f). As the number of growth cycles increased, the nanorods became longer while remaining in the form of vertically well-aligned arrays without any lateral coalescence in the measuring space. Surprisingly, the diameter of the nanorods hardly changed from the bottom to the top, as indicated by the yellow arrows in Fig. 5f. This strongly indicates that the constant growth kinetics were maintained over the entire growth process. For a more quantitative analysis, the height and unit growth volume are respectively plotted in Figs. 5g and 5h. Here, we defined the unit growth volume as total volume/growth time. Owing to the high aspect ratio of each nanorod, the volume of each nanorod was simply approximated using the volume formula for a hexagonal prism, $V = (3\sqrt{3}/2)\times a \times h$, where a is half of the in-plane length in the $\langle 11\bar{2}0 \rangle$ direction from the center position (i.e., a base edge) and h is the height of the prism. For the hole diameter of 190 nm, a monotonic increase in the c-plane height was observed, while the increase in height for the hole diameter of 460 nm was much slower, as shown in Fig. 5g. Hence, the height difference gradually increased with the number of pulsed-mode cycles. A large difference was also found in the unit growth volume, as shown in Fig. 5h. The unit growth volume for the hole diameter of 190 nm slowly decreased and converged to ~2.7 $\mu m^3/h$ as the number of cycles increased. On the other hand, that for the hole diameter of 460 nm almost linearly decreased. It is speculated that the high unit growth volume at a low number of cycles (< 300) is due to the higher probability of assisted adatom incorporation from surface diffusion at the beginning of growth.[46] As the height of the nanorods increases, vapor-phase atoms might mainly contribute to the growth process, thereby reducing the growth rate. For the smaller hole diameter, the growth time required to form a monolayer might be shorter than that for the

CrystEngComm Accepted Manuscript

larger hole diameter, thereby resulting in highly elongated nanorods. Figure 5i exhibits the kinetic Wulff plot for GaN nanorods grown with 1000 cycles, where the interpolation parameters were acquired in a similar manner to that shown in Fig. S4. As is evident from Fig. 4c, much deeper cusps were observed in the $\langle 10\bar{1}0 \rangle$ direction than in the other directions for the both hole diameters. The nanorods with the smaller diameter exhibited a much higher growth rate comparable to that of typical 2D film growth. The greatest height among all the samples was reached ~10 μm after 1000 cycles. Considering that a typical 2D GaN layer on an AlN/Si platform suffers from severe cracking and its crack-free length is limited to within ~500 nm owing to the large thermal mismatch with Si, this result is encouraging regarding the realization of high-quality and very long GaN nanorods on Si, even without strain buffer layers such as an AlGaN stack.[47] Indeed, the diameter of the nanorods was critically affected by that of the hole openings since lateral growth was almost completely suppressed in this study. Similar behavior has been observed elsewhere, where the nanorod diameter was similar to the initial size of the nuclei.[23] This should allow the growth of nanorods with much smaller diameters provided a mask with much smaller openings is available. Therefore, to grow GaN nanorods with a higher aspect ratio, it is necessary to reduce the opening size; thus, the time required for the formation of a monolayer should be reduced under the same diffusion flux conditions. Elongated GaN nanorods can ultimately be grown by more advanced and high-resolution patterning techniques such as nanosphere patterning, diblock copolymer lithography, rapid convective deposition, and so forth.[48–50]

Conclusion

In this paper, we reported arrays of highly elongated and well-aligned GaN nanorods on Si-based templates by MOCVD with the pulsed-mode approach. Even though a low-quality and ultrathin AlN layer was used as a seed layer instead of a commonly used high (or middle)-quality and thick GaN layer, it played an effective role in growing high-quality GaN nanorod arrays with high geometric precision. According to the many observations of the growth kinetic behaviors, the optimized pulsed-mode growth exhibited the features of N-rich 2D film growth. The equilibrium shape of the grown

CrystEngComm Accepted Manuscript

nanostructures accurately reflected the controlled growth velocity of the main growth orientations, particularly the highly suppressed growth rate along the lateral direction. Owing to their volumetric stability, the height of the nanorods increased as the diameter of the mask openings decreased. Therefore, we expect that the pulsed-mode approach will serve as an effective method of growing GaN nanorod arrays for a variety of mother materials. Furthermore, the growth of even longer GaN nanorods might be possible by more advanced patterning techniques.

Acknowledgments

The authors (S.-Y. Bae and K. Lekhal) were an international research fellow of the Japan society for the promotion of science (JSPS) and the author (B.O. Jung) was funded by a monbukagakusho scholarship from the ministry of education, culture, sports, science and technology (MEXT) of Japan. This work was supported by JSPS KAKENHI Grant Numbers 2604366, 25000011, and 24686041.

CrystEngComm Accepted Manuscript

References

1 M. S. Dresselhaus, Y.-M. Lin, O. Rabin, M. R. Black, J. Kong and G. Dresselhaus, in *Springer Handbook of Nanotechnology*, Springer, 2010, pp. 119–167.

2 D. Zubia and S. D. Hersee, *J. Appl. Phys.*, 1999, **85**, 6492–6496.

3 A. Waag, X. Wang, S. Fündling, J. Ledig, M. Erenburg, R. Neumann, M. Al Suleiman, S. Merzsch, J. Wei, S. Li and others, *Phys. Status Solidi C*, 2011, **8**, 2296–2301.

4 Y.-H. Ko, J.-H. Kim, L.-H. Jin, S.-M. Ko, B.-J. Kwon, J. Kim, T. Kim and Y.-H. Cho, *Adv. Mater.*, 2011, **23**, 5364–5369.

5 B. O. Jung, S.-Y. Bae, S. Y. Kim, S. Lee, J. Y. Lee, D.-S. Lee, Y. Kato, Y. Honda and H. Amano, *Nano Energy*, 2015, **11**, 294–303.

6 Y. J. Hong, C.-H. Lee, A. Yoon, M. Kim, H.-K. Seong, H. J. Chung, C. Sone, Y. J. Park and G.-C. Yi, *Adv. Mater.*, 2011, **23**, 3284–3288.

7 H. Sekiguchi, K. Kishino and A. Kikuchi, *Appl. Phys. Lett.*, 2010, **96**, 231104.

8 T.-W. Yeh, Y.-T. Lin, L. S. Stewart, P. D. Dapkus, R. Sarkissian, J. D. O'Brien, B. Ahn and S. R. Nutt, *Nano Lett.*, 2012, **12**, 3257–3262.

9 R. K. Joshi and J. J. Schneider, *Chem. Soc. Rev.*, 2012, **41**, 5285–5312.

10 H.-M. Kim, D. S. Kim, Y. S. Park, D. Y. Kim, T. W. Kang and K. S. Chung, *Adv. Mater.*, 2002, **14**, 991–993.

11 R. S. Wagner and W. C. Ellis, *Appl. Phys. Lett.*, 1964, 89–90.

12 K. Lekhal, G. Avit, Y. André, A. Trassoudaine, E. Gil, C. Varenne, C. Bougerol, G. Monier and D. Castelluci, *Nanotechnology*, 2012, **23**, 405601.

13 D. Tsivion, M. Schvartzman, R. Popovitz-Biro, P. von Huth and E. Joselevich, *Science*, 2011, **333**, 1003–1007.

14 K. Hiramatsu, K. Nishiyama, A. Motogaito, H. Miyake, Y. Iyechika and T. Maeda, *Phys. Status Solidi A*, 1999, **176**, 535–543.

15 H. J. Fan, P. Werner and M. Zacharias, *small*, 2006, **2**, 700–717.

16 D. S. Kim, R. Ji, H. J. Fan, F. Bertram, R. Scholz, A. Dadgar, K. Nielsch, A. Krost, J. Christen, U.

CrystEngComm Accepted Manuscript

Gösele and others, *small*, 2007, **3**, 76–80.

17 L. Liu and J. H. Edgar, *Mater. Sci. Eng. R Rep.*, 2002, **37**, 61–127.

18 H. Sekiguchi, K. Kishino and A. Kikuchi, *Appl. Phys. Lett.*, 2010, **96**, 231104.

19 S. F. Li, S. Fuendling, X. Wang, S. Merzsch, M. A. M. Al-Suleiman, J. D. Wei, H.-H. Wehmann, A. Waag, W. Bergbauer and M. Strassburg, *Cryst. Growth Des.*, 2011, **11**, 1573–1577.

20 S. D. Hersee, X. Sun and X. Wang, *Nano Lett.*, 2006, **6**, 1808–1811.

21 T.-Y. Tang, W.-Y. Shiao, C.-H. Lin, K.-C. Shen, J.-J. Huang, S.-Y. Ting, T.-C. Liu, C. C. Yang, C.-L. Yao, J.-H. Yeh and others, *J. Appl. Phys.*, 2009, **105**, 23501.

22 Y.-T. Lin, T.-W. Yeh, Y. Nakajima and P. D. Dapkus, *Adv. Funct. Mater.*, 2014, **24**, 3162–3171.

23 S.-Y. Bae, J.-Y. Lee, J.-H. Min and D.-S. Lee, *Appl. Phys. Express*, 2013, **6**, 075501.

24 S. D. Hersee, A. K. Rishinaramangalam, M. N. Fairchild, L. Zhang and P. Varangis, *J. Mater. Res.*, 2011, **26**, 2293–2298.

25 Y.-T. Lin, T.-W. Yeh and P. D. Dapkus, *Nanotechnology*, 2012, **23**, 465601.

26 B. O. Jung, S.-Y. Bae, Y. Kato, M. Imura, D.-S. Lee, Y. Honda and H. Amano, *CrystEngComm*, 2014, **16**, 2273–2282.

27 H.-S. Chen, Y.-F. Yao, C.-H. Liao, C.-G. Tu, C.-Y. Su, W.-M. Chang, Y.-W. Kiang and C. C. Yang, *Opt. Lett.*, 2013, **38**, 3370–3373.

28 T. Mitsunari, H. J. Lee, Y. Honda and H. Amano, *J. Cryst. Growth*, 2015, **431**, 60–63.

29 L. A. Reichertz, I. Gherasoiu, K. M. Yu, V. M. Kao, W. Walukiewicz and J. W. Ager III, *Appl. Phys. Express*, 2009, **2**, 122202.

30 K. Tomioka, M. Yoshimura and T. Fukui, *Nature*, 2012, **488**, 189–192.

31 K. Hiramatsu, K. Nishiyama, A. Motogaito, H. Miyake, Y. Iyechika and T. Maeda, *Phys. Status Solidi A*, 1999, **176**, 535–543.

32 F. Shahedipour-Sandvik, J. Grandusky, A. Alizadeh, C. Keimel, S. P. Ganti, S. T. Taylor, S. F. LeBoeuf and P. Sharma, *Appl. Phys. Lett.*, 2005, **87**, 233108.

33 T. Kim, J. Kim, M.-S. Yang, S. Lee, Y. Park, U.-I. Chung and Y. Cho, *Appl. Phys. Lett.*, 2010, **97**, 241111.

CrystEngComm Accepted Manuscript

34 V. Jindal and F. Shahedipour-Sandvik, *J. Appl. Phys.*, 2009, **106**, 083115.

35 Q. Sun, C. D. Yerino, T. S. Ko, Y. S. Cho, I.-H. Lee, J. Han and M. E. Coltrin, *J. Appl. Phys.*, 2008, **104**, 093523.

36 K. Xu, N. Yano, A. w. Jia, A. Yoshikawa and K. Takahashi, *Phys. Status Solidi B*, 2001, **228**, 523–527.

37 C. Kisielowski, J. Krüger, S. Ruvimov, T. Suski, J. W. Ager III, E. Jones, Z. Liliental-Weber, M. Rubin, E. R. Weber, M. D. Bremser and others, *Phys. Rev. B*, 1996, **54**, 17745.

38 S.-M. Ko, J.-H. Kim, Y.-H. Ko, Y. H. Chang, Y.-H. Kim, J. Yoon, J. Y. Lee and Y.-H. Cho, *Cryst. Growth Des.*, 2012, **12**, 3838–3844.

39 K. Kishino and S. Ishizawa, *Nanotechnology*, 2015, **26**, 225602.

40 I. Petrov, P. B. Barna, L. Hultman and J. E. Greene, *J. Vac. Sci. Technol. A*, 2003, **21**, S117–S128.

41 H. Amano, N. Sawaki, I. Akasaki and Y. Toyoda, *Appl. Phys. Lett.*, 1986, **48**, 353–355.

42 D. Tham, C.-Y. Nam and J. E. Fischer, *Dep. Pap. MSE*, 2006, 114.

43 D. D. Koleske, A. E. Wickenden, R. L. Henry, W. J. DeSisto and R. J. Gorman, *J. Appl. Phys.*, 1998, **84**.

44 D. Du, D. J. Srolovitz, M. E. Coltrin and C. C. Mitchell, *Phys. Rev. Lett.*, 2005, **95**, 155503.

45 V. Jindal, *Development of III-nitride nanostructures by metal-organic chemical vapor deposition*, ProQuest, 2008.

46 T. Gotschke, T. Schumann, F. Limbach, T. Stoica and R. Calarco, *Appl. Phys. Lett.*, 2011, **98**, 103102.

47 D. Zhu, D. J. Wallis and C. J. Humphreys, *Rep. Prog. Phys.*, 2013, **76**, 106501.

48A. R. Madaria, M. Yao, C. Chi, N. Huang, C. Lin, R. Li, M. L. Povinelli, P. D. Dapkus and C. Zhou, *Nano Lett.*, 2012, **12**, 2839–2845.

49 X.-H. Li, P. Zhu, G. Liu, J. Zhang, R. Song, Y.-K. Ee, P. Kumnorkaew, J. F. Gilchrist and N. Tansu, *Disp. Technol. J. Of*, 2013, **9**, 324–332.

50 T. F. Kuech and L. J. Mawst, *J. Phys. Appl. Phys.*, 2010, **43**, 183001.

CrystEngComm Accepted Manuscript

Figure captions

Figure 1. Cross-sectional SEM images of nanostructures grown with different NH_3 injection times (t_2) and TMG injection times (t_1). (a) $t_2 = 5$ s, (b) $t_2 = 10$ s, (c) $t_2 = 20$ s, (d) $t_1 = 3.75$ s, (e) $t_1 = 5$ s, (f) $t_1 = 7.5$ s, and (g) $t_1 = 15$ s. Note that 150 pulsed-mode cycles were performed for all cases and PMGR was controlled by varying the ratio of t_2 to t_1 with a fixed interruption time (t_3 and $t_4 = 1$ s).

Figure 2. PL spectra obtained by (a) varying the NH_3 injection time (t_2) while fixing t_1 (5 s) and (b) varying the TMG injection time (t_1) while fixing t_2 (15 s), where 150 pulsed-mode cycles were carried out. Cross-sectional DF-TEM images of GaN nanorods grown on AlN/Si template with (c) small hole diameter of 230 nm and (d) large hole diameter of 460 nm. (e) XRD omega scan of GaN nanorods with PMGR of 3. HR images of (f) AlN/Si interface, (g) GaN/AlN interface, and (h) middle of GaN nanorods. Note that the locations of the images in (f)–(h) are indicated in Fig. 2c. The inset of Fig. 2h is an SAED pattern obtained from the middle of the GaN nanorods.

Figure 3. (a)–(c) SEM images of nanostructures grown while changing the V/III ratio. In the inset of each SEM image is a schematic illustrating the grown structures and showing the relative growth lengths with arrows. Note that a yellow arrow indicates an enhanced growth length compared with other directions. (d) Ratio of N to Ga desorption (k_N/k_{Ga}) as a function of temperature (blue curve) and V/III ratios used in this experiment (red circles). (e) Top-view SEM image of GaN nanorods. (f) EBSD pole figures in $\{0001\}, \{10\bar{1}0\}$, and $\{10\bar{1}1\}$ planes. (g) Histogram of tilted deviation angle for in-plane (a-plane) and out-of-plane (c-plane) nanorods.

Figure 4. Actual SEM images (left) and kinetic Wulff plots (right) for representative equilibrium shapes: (a) hexagonal pyramid, (b) short nanorod, and (c) long nanorod. Full cusps were found in three directions, i.e., $[0001]$, $[10\bar{1}1]$, and $[10\bar{1}0]$. Note that a much deeper cusp is observed in the $[10\bar{1}0]$ direction for the elongated nanorod structure. Scale bar = 250 nm.

CrystEngComm Accepted Manuscript

Figure 5. SEM images of GaN nanorods grown with 164 cycles, 300 cycles, and 1000 cycles for hole diameters of (a–c) 460 nm and (d–f) 190 nm. (g) Height and (h) unit growth volume of GaN nanorods as a function of number of pulsed-mode cycles. Here, D is the diameter of the opening holes. (i) Kinetic Wulff plots of GaN nanorods after 1000 cycles for hole diameters 190 nm (red) and 460 nm (blue). Note that the deepest cusp appears in the $[10\bar{1}0]$ direction, indicating effectively suppressed lateral growth.

CrystEngComm Accepted Manuscript

Figures

Figure 1

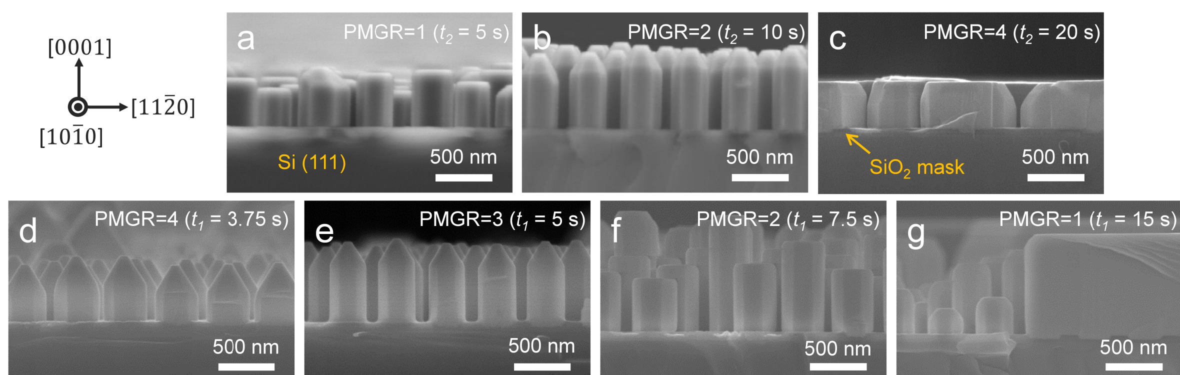

CrystEngComm Accepted Manuscript

Figure 2

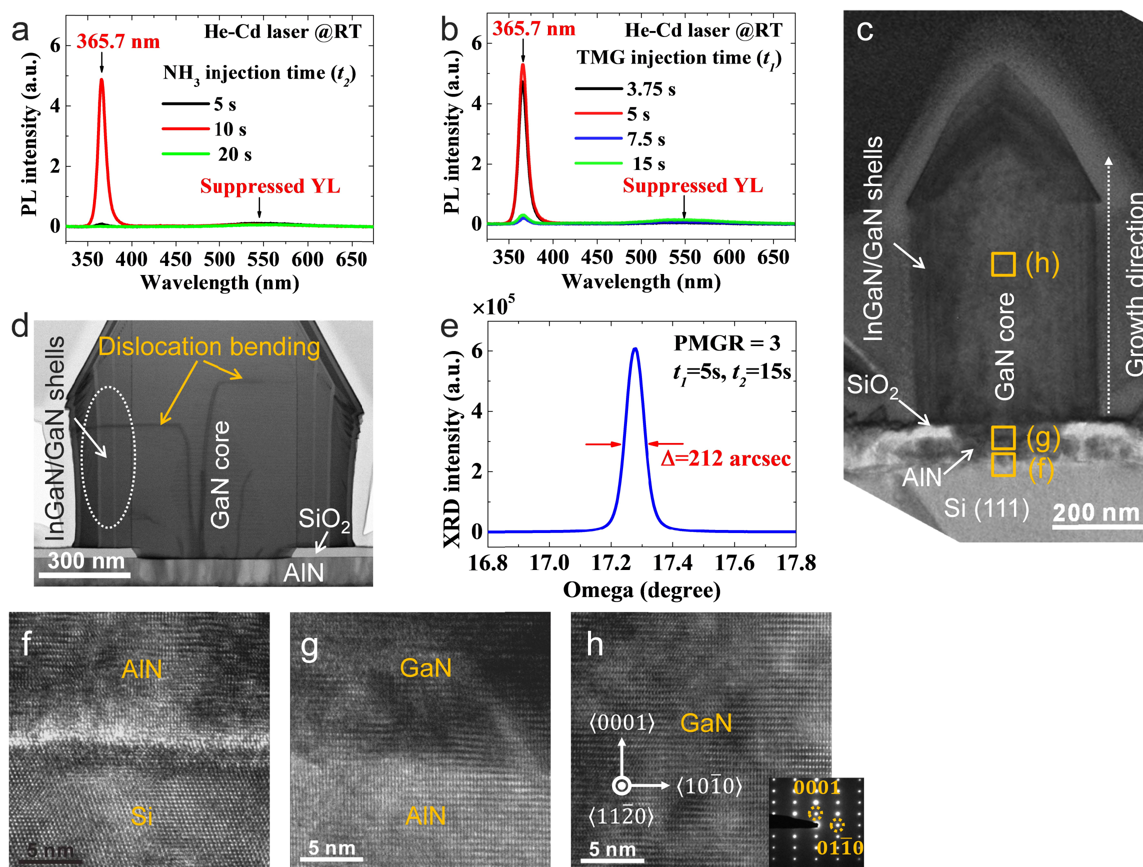

CrystEngComm Accepted Manuscript

Figure 3

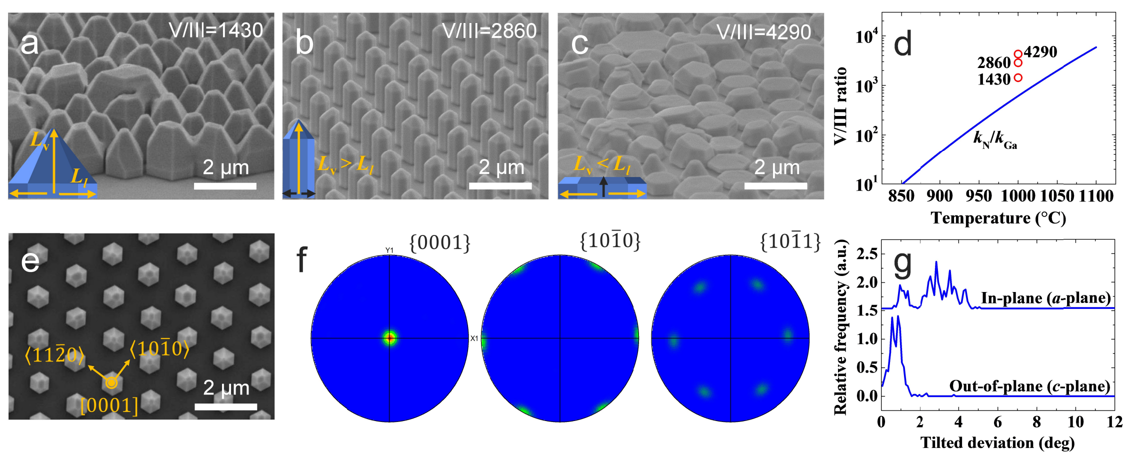

CrystEngComm Accepted Manuscript

Figure 4

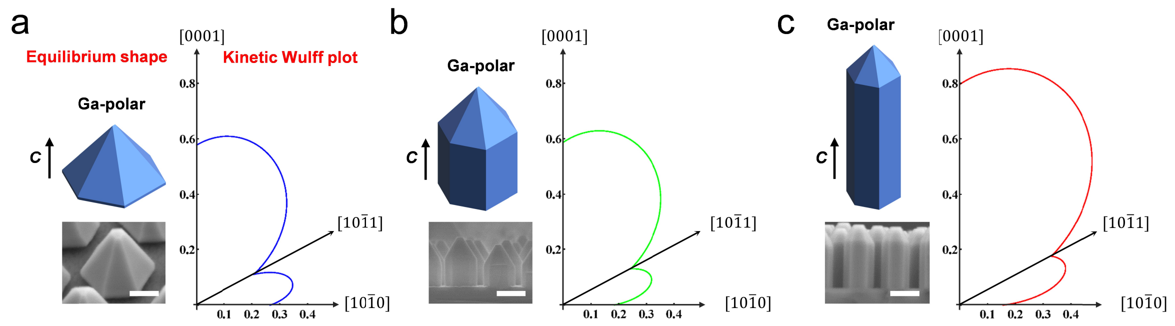

CrystEngComm Accepted Manuscript

Figure 5

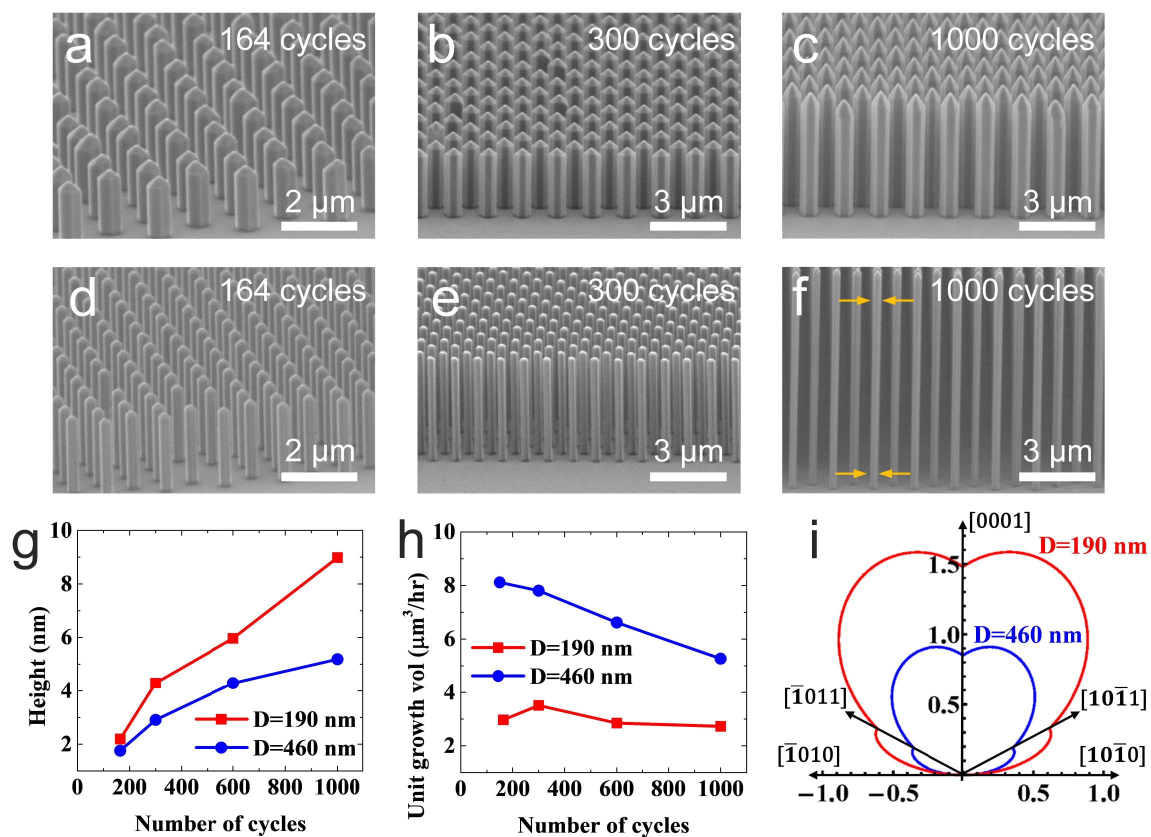

CrystEngComm Accepted Manuscript